Journal of Fluids and Structures (1997) **11,** 367–393

OVERFLOW-INDUCED VIBRATION OF A WEIR COUPLED WITH SLOSHING IN A DOWNSTREAM TANK

D. Lu,*‡ A. Takizawa† and S. Kondo*
** Department of Quantum Engineering and Systems Science, University of Tokyo Tokyo 113, Japan*
† Nuclear Power R&D Center, Tokyo Electric Power Company Yokohama 230, Japan

(Received 27 October 1994 and in finally revised form 10 January 1997)

This paper presents a new analytical method for the analysis of overflow-induced vibration of a weir. In this method, the potential separation technique and Laplace transform are used to solve the equation of potential flow and the governing equation of the fluid-structure coupled system respectively, and an overflow model is developed to describe the behavior of the overflow falling into the downstream tank. The analytical results show good agreement with the numerical ones. The mechanism of the overflow-induced vibration is clarified and measures to suppress or alleviate such vibration are also proposed.

1. INTRODUCTION

In this paper a special phenomenon will be discussed, which is the overflow-induced vibration of an elastic weir coupled with the sloshing of free-surface coolant in a downstream tank. This phenomenon was first observed in the French Demonstration LMFBR (liquid metal cooled fast breeder reactor) "Super Phenix (SPX)" (Aita *et al.* 1986). Because the coolant coming out of the reactor core has a very high temperature in the LMFBR, a thin-walled weir was installed to form a forced circulation loop of cold sodium between the weir and the reactor wall to protect the reactor wall from excessive thermal stress (see Figure 1). However, undesirable vibration of the weir was observed in the pre-operation stage of the SPX. It is important for the safety assessment of the LMFBR to clarify the mechanism of this overflow-induced vibration.

The experiments of Aita *et al.* (1986) found that there are two modes of vibration: a "sloshing mode", where the vibration is coupled with the sloshing of coolant in the downstream region, and a "fluid-elastic mode", where no sloshing occurs. Eguchi & Tanaka (1990) and Kaneko *et al.* (1991) performed experiments in either rectangular or cylindrical tanks using flexible weirs. Fujita *et al.* (1992, 1993) performed three-dimensional (3-D) experiments using a $\frac{1}{10}$-scale and $\frac{1}{5}$-scale weir model of the thermal shield of the Japanese Demonstration LMFBR. Although the vibration observed in SPX is a 3-D phenomenon in concentric cylindrical vessels, in a basic study essentially

‡ Present affiliation: O-arai Engineering Center, Power Reactor and Nuclear Fuel Development Corporation, Ibaraki 311-13, Japan.

0889–9746/97/040367 + 27 $25.00/fl970084

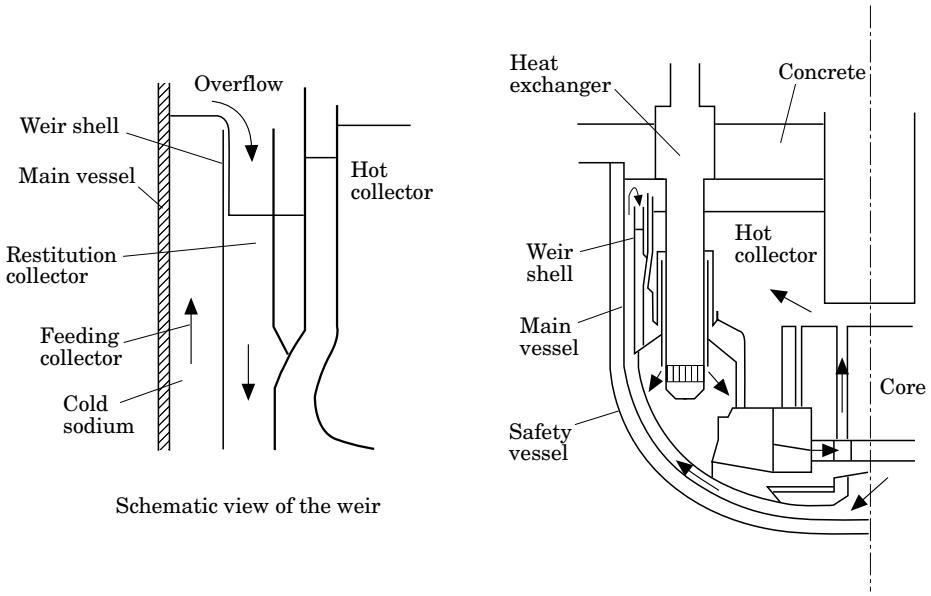

Figure 1. Layout of French LMFBR Super Phenix (Aïta *et al.* 1986).

the same phenomenon was found in a 2-D rectangular tank having a spring-supported rotatable rigid weir (see Figure 2) by Fukuie & Hara (1989).

Since the experimental method has various limitations in measuring physical variables under the dynamic movement of a free surface or walls, a theoretical analysis as well as numerical analysis are necessary to understand the mechanism of this vibration. From the viewpoint of both numerical and theoretical analysis, Fukuie & Hara's experiment is the best one because it is the simplest among them, being purely

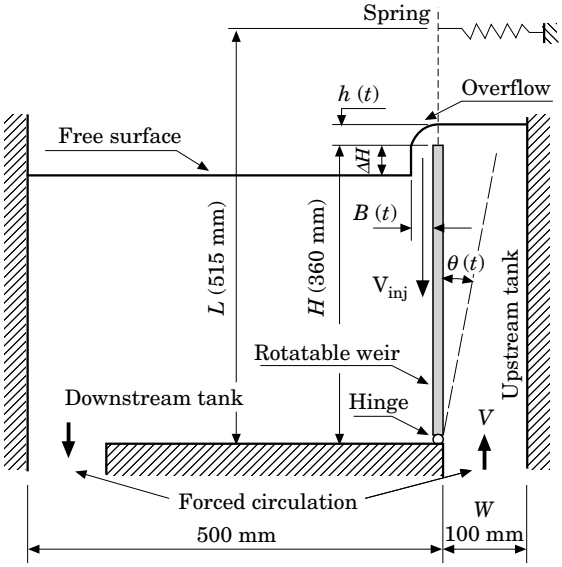

Figure 2. Experimental apparatus of Fukuie & Hara (1989).

a 2-D experiment. The spring-supported rotatable rigid weir in their experiment also facilitates the analysis because it does not involve the additional complexity of the bending of the weir.

Eguchi & Tanaka (1990), Hara & Suzuki (1992), and Kaneko *et al.* (1993) have presented their theoretical models for the present problem using the conventional analytical method of modal analysis. In their models, the pressure boundary assumption at the inlet of the overflow into the downstream tank was used, which assumes that all the kinetic energy of the overflow is transformed into pressure when the overflow hits the free surface in the downstream tank. However, this assumption may not be very realistic.

Different from the modal analysis, we adopted a potential separation technique in order to use the more natural boundary condition at the inlet of the overflow into the downstream tank. The potential separation technique was developed by Aslam *et al.* (1979) and Fujita *et al.* (1985) for analysis of the seismic response of sloshing in a rigid tank. In the present study we extend this technique by incorporating a spring-supported weir module. Formulation of this new analytical method is introduced in Section 2. Validation of the newly extended method is presented in Section 3 by comparison with numerical results. Application of the present analytical method to Fukuie & Hara's experiment is effected in Section 4, where we give a natural velocity boundary model to the inlet of the overflow into the downstream tank. Conclusions are presented in Section 5.

2. FORMULATION OF THEORETICAL METHOD

2.1. Flow Velocity Potential in a Tank Having a Movable Wall

We begin the study by solving the flow velocity potential in a tank having a movable wall as shown in Figure 3, where the spring-supported wall moves in two ways: translation and rotation. The translation case is simple, easy to solve, and it is also easy for us to understand the physical meaning of the derived formulae. The rotation case is more realistic because it is the manner of movement in Fukuie & Hara's experiment. From here on, an $\{x, z\}$ coordinate system is used, with the origin at the left end of the stationary free surface, as shown in Figure 3.

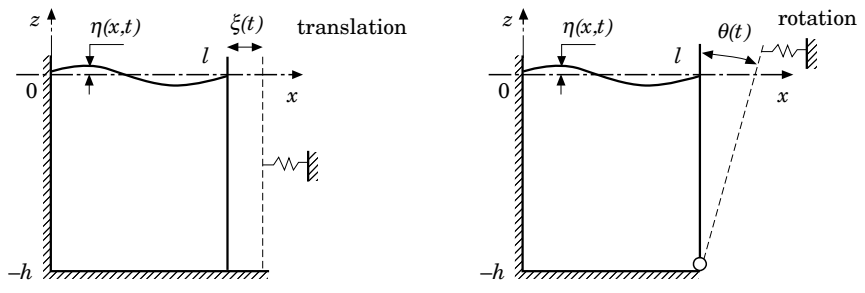

(a) Translation case (b) Rotation case

Figure 3. Fluid motion in a tank having a spring-supported movable wall which moves in two different ways, (a) and (b).

2.1.1. *Translation case*

We start with the translation case. By assuming the free-surface liquid as a potential flow, we can describe the governing equation of the sloshing using flow velocity potential ϕ as follows:

$$\frac{\partial^2\phi}{\partial x^2}+\frac{\partial^2\phi}{\partial z^2}=0, \qquad \text{(equation of continuity)} \tag{1}$$

with the boundary conditions

$$\left.\frac{\partial\phi}{\partial x}\right|_{x=0}=0, \qquad \left.\frac{\partial\phi}{\partial x}\right|_{x=l}=\dot{\xi}(t), \qquad \text{(at the walls)} \tag{2}$$

$$\left.\frac{\partial\phi}{\partial z}\right|_{z=-h}=0, \qquad \text{(at the bottom)}, \tag{3}$$

and

$$\frac{\partial^2\phi}{\partial t^2}+g\left.\frac{\partial\phi}{\partial z}\right|_{z=0}=0, \qquad \text{(at the free surface)} \tag{4}$$

where l, h, g and $\xi(t)$ are, respectively, the width and the depth of the tank, the acceleration of gravity, and the displacement of the right wall from its original position; the dot denotes differentiation with time.

In order to solve the nonhomogeneous boundary condition at the movable wall, we need to separate ϕ into ϕ_F and ϕ_1: ϕ_F relating to the movement of the right wall with no sloshing of the free surface, and ϕ_1 relating only to the sloshing of the free surface.

ϕ_F is governed by equations (1)–(3) and the boundary condition at the free surface,

$$\left.\frac{\partial\phi_F}{\partial z}\right|_{z=0}=-\frac{h}{l}\dot{\xi}(t). \tag{5}$$

A special solution of ϕ_F can be chosen as

$$\phi_F=\frac{x^2-(z+h)^2}{2l}\dot{\xi}(t). \tag{6}$$

By subtracting ϕ_F from the equation set (1)–(4), we can derive the equation set for ϕ_1, which is the same as (1)–(4) except for the boundary conditions at the movable wall and at the free surface; they should be replaced by the following equations, respectively:

$$\left.\frac{\partial\phi_1}{\partial x}\right|_{x=l}=0, \qquad \text{and} \quad \frac{\partial^2\phi_1}{\partial t^2}+g\left.\frac{\partial\phi_1}{\partial z}\right|_{z=0}=-g\left.\frac{\partial\phi_F}{\partial z}\right|_{z=0}-\left.\frac{\partial^2\phi_F}{\partial t^2}\right|_{z=0}. \tag{7}$$

As a solution of ϕ_1, we assume the following form, which is a sum of sloshing in nth mode,

$$\phi_1=\sum_{n=0}^{\infty}\cos k_n x\cosh k_n(z+h)T_n(t), \qquad n=0, 1, 2, \ldots \tag{8}$$

where $T_n(t)$ is unknown and $k_n=n\pi/l$ is a wavenumber.

By substituting equations (6) and (8) into (7), we can obtain the following equation for $T_n(t)$:

$$\sum_{n=0}^{\infty} \cos k_n x \cosh k_n h[\ddot{T}(t) + \omega_n^2 T_n(t)] = \frac{gh}{l}\dot{\xi}(t) - \frac{x^2 - h^2}{2l}\dddot{\xi}(t), \tag{9}$$

where $\omega_n = \sqrt{gk_n \tanh k_n h}$ is the natural frequency of sloshing in a rigid tank. Then we expand x^2 in the above equation by Fourier series in the range $[0, l]$ as follows;

$$x^2 = \frac{l^2}{3} + \sum_{n=1}^{\infty} a_n \cos k_n x, \tag{10}$$

where $a_n = (2/l)\ \int_0^l x^2 \cos k_n x\, \mathrm{d}x = 4(-1)^n/k_n^2,\ (n \neq 0)$. Using equation (10), equation (9) can be rewritten as follows:

$$\sum_{n=0}^{\infty} \cos k_n x \cosh k_n h[\ddot{T}(t) + \omega_n^2 T_n(t)] = \left[\frac{gh}{l}\dot{\xi}(t) + \frac{h^2}{2l}\dddot{\xi}(t) - \frac{l}{6}\dddot{\xi}(t)\right]$$

$$-\sum_{n=1}^{\infty} \frac{a_n}{2l}\cos k_n x\dddot{\xi}(t) = \left[\frac{gh}{l}\alpha + \frac{h^2}{2l} - \frac{l}{6}\right]\dddot{\xi}(t) - \sum_{n=1}^{\infty} \frac{a_n}{2l}\cos k_n x\dddot{\xi}(t), \tag{11}$$

where α is a constant. From equation (11), we can obtain the following equation for each n:

$$\ddot{T}(t) + \omega_n^2 T_n(t) = -\frac{\beta_n}{\cosh k_n h}\dddot{\xi}(t), \tag{12}$$

where $\beta_0 = -[(gh/l)\alpha + h^2/2l - \frac{1}{6}l]$ and $\beta_n = a_n/2l,\ (n \neq 0)$. Equation (12) gives the following solution for $T_n(t)$:

$$T_n(t) = -\frac{\beta_n}{\omega_n \cosh k_n h}\int_0^t \dddot{\xi}(\tau) \sin \omega_n(t - \tau)\, \mathrm{d}\tau. \tag{13}$$

Finally, from equations (6), (8) and (13) we can obtain the following explicit expression for the velocity potential ϕ:

$$\phi = \phi_F + \phi_1 = \frac{x^2 - (z + h)^2}{2l}\dot{\xi}(t)$$

$$-\sum_{n=0}^{\infty} \frac{\beta_n}{\omega_n \cosh k_n h}\cos k_n x \cosh k_n(z + h)\int_0^t \dddot{\xi}(\tau) \sin \omega_n(t - \tau)\, \mathrm{d}\tau. \tag{14}$$

2.1.2. *Rotation case*

The only difference between the set of governing equations for the rotation and the translation cases is the right-wall boundary condition. The second of equations (2) should be replaced by

$$\left.\frac{\partial \phi}{\partial x}\right|_{x=l} = (z + h)\dot{\theta}(t), \tag{15}$$

where $\theta(t)$ denotes rotation of the wall measured from the vertical position. Similarly

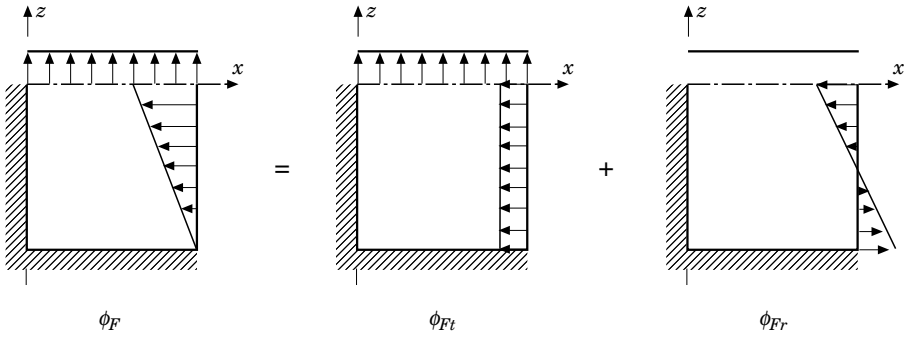

Figure 4. Movement separation for a rotatable wall.

to the translation case, ϕ is separated into ϕ_F and ϕ_1, and ϕ_F is determined by the equation set which is the same as equations (1)–(4), except for the boundary conditions at the movable wall and at the free surface, which are

$$\left.\frac{\partial \phi_F}{\partial x}\right|_{x=l} = (z+h)\dot{\theta}(t), \qquad \text{and} \quad \left.\frac{\partial \phi_F}{\partial z}\right|_{z=0} = -\frac{h^2}{2l}\dot{\theta}(t). \tag{16}$$

As shown in Figure 4, we further separate ϕ_F into the translation part ϕ_{Ft} and the rotation part ϕ_{Fr}; ϕ_{Ft} is governed by the equation set which is the same as (1)–(4), except for the boundary conditions at the movable wall and at the free surface, which are

$$\left.\frac{\partial \phi_{Ft}}{\partial x}\right|_{x=l} = \frac{h}{2}\dot{\theta}(t), \qquad \text{and} \quad \left.\frac{\partial \phi_{Ft}}{\partial z}\right|_{z=0} = -\frac{h^2}{2l}\dot{\theta}(t), \tag{17}$$

whose special solution is

$$\phi_{Ft} = \frac{h}{2}\frac{x^2-(z+h)^2}{2l}\dot{\theta}(t). \tag{18}$$

Meanwhile, ϕ_{Fr} is related to the rotation of the right wall without changing the water level and is determined by equation set (1)–(4) again, except for the boundary conditions at the movable wall and at the free surface, which are

$$\left.\frac{\partial \phi_{Fr}}{\partial x}\right|_{x=l} = \left(z+\frac{h}{2}\right)\dot{\theta}(t), \qquad \text{and} \quad \left.\frac{\partial \phi_{Fr}}{\partial z}\right|_{z=0} = 0. \tag{19}$$

We now assume the following expansion for ϕ_{Fr}:

$$\phi_{Fr} = \sum_{m=1}^{\infty} b_m \cosh \lambda_m x \sin \lambda_m (z+\tfrac{1}{2}h)\dot{\theta}(t), \qquad m = 1, 2, 3, \ldots \tag{20}$$

where $\lambda_m = [(2m-1)/h]\pi$. Then, by substituting equation (20) into (19), we can obtain the following expression for b_m:

$$b_m = \frac{4(-1)^{m-1}}{h\lambda_m^3 \sinh \lambda_m l}. \tag{21}$$

Applying a similar process to equations (7) through (13) in the translation case, we

can obtain the potential ϕ_1 in the rotation case as follows [for the details, please refer to appendix II.A in Lu (1995)]:

$$\phi_1 = -\sum_{n=0}^{\infty} \frac{\beta_n}{\omega_n \cosh k_n h} \cosh k_n x \cosh k_n (z+h) \int_0^t \dddot{\theta}(\tau) \sin \omega_n (t-\tau)\, \mathrm{d}\tau, \tag{22}$$

where β_n in the present case is expressed as follows:

$$\begin{aligned}\beta_n &= \frac{a_n}{2l}\frac{h}{2}\left[1 + \frac{8}{\pi^2}\left(\sum_{m=1}^{\infty}\frac{1}{(2m-1)^2} - \sum_{m=1}^{\infty}\frac{1}{(2m-1)^2 + (nh/l)^2}\right)\right] \\ &= \frac{a_n}{2l}\frac{h}{2}\left[2 - \frac{4l}{nh\pi}\left(\frac{e^{(nh\pi/l)}}{\sinh(nh\pi/l)} - \frac{e^{(nh\pi/2l)}}{2\sinh(nh\pi/2l)} - \frac{1}{2}\right)\right].\end{aligned} \tag{23}$$

Finally, we obtain the explicit expression for ϕ from equations (18), (20) and (22):

$$\phi = \phi_{Fl} + \phi_{Fr} + \phi_1. \tag{24}$$

2.1.3. *Growth rate of sloshing excited by the movable wall*

According to the Bernoulli equation the water level is expressed as follows:

$$\eta = -\frac{1}{g}\frac{\partial \phi}{\partial t}\bigg|_{z=0}. \tag{25}$$

Substituting equation (14) into (25), we obtain

$$\begin{aligned}\eta &= -\frac{1}{g}\left[\frac{x^2 - h^2}{2l}\ddot{\xi}(t) - \sum_{n=1}^{\infty}\beta_n \cos k_n x \int_0^t \dddot{\xi}(\tau)\cos\omega_n(t-\tau)\,\mathrm{d}\tau\right] \\ &= -\frac{1}{g}\left[\frac{\frac{1}{3}l^2 - h^2}{2l}\ddot{\xi}(t) + \sum_{n=1}^{\infty}\beta_n \cos k_n x \ddot{\xi}(t)\right. \\ &\quad \left. - \sum_{n=1}^{\infty}\beta_n \cos k_n x\left(\ddot{\xi}(t) - \omega_n\int_0^t \ddot{\xi}(\tau)\sin\omega_n(t-\tau)\,\mathrm{d}\tau\right)\right] \\ &= -\frac{1}{g}\left[\frac{\frac{1}{3}l^2 - h^2}{2l}\ddot{\xi}(t) + \sum_{n=1}^{\infty}\omega_n\beta_n \cos k_n x \int_0^t \ddot{\xi}(\tau)\sin\omega_n(t-\tau)\,\mathrm{d}\tau\right].\end{aligned} \tag{26}$$

When the sloshing is in the nth mode, and the right wall is oscillated according to

$$\dot{\xi}(t) = D\cos\omega_n t, \tag{27}$$

the water level is obtained as follows:

$$\begin{aligned}\eta &= \frac{1}{g}\left[\frac{\frac{1}{3}l^2 - h^2}{2l} D\omega_n \sin\omega_n t + \beta_n \cos k_n x D\omega_n^2 \int_0^t \sin\omega_n\tau \sin\omega_n(t-\tau)\,\mathrm{d}\tau)\right] \\ &= \frac{D\omega_n}{2gl}\left(\frac{1}{3}l^2 - h^2\right)\sin\omega_n t + \frac{\beta_n D\omega_n^2}{2g}\left(\frac{\sin\omega_n t}{\omega_n} - t\cos\omega_n t\right)\cos k_n x.\end{aligned} \tag{28}$$

So the growth rate (GR) of water level can be calculated as

$$\mathrm{GR} = \left|\frac{\beta_n D\omega_n^2}{2g}\right|. \tag{29}$$

In the same way, it is found that the growth rate in the rotation case can also be expressed by equation (29).

2.2. Fluid–Wall Interaction in a Tank Having Spring-supported Movable Wall

We next solve the fluid-wall interaction in a tank having a spring-supported movable wall as shown in Figure 3.

2.2.1. *Translation case*

The equation of motion of a spring-supported wall can be written as follows:

$$m\ddot{\xi}(t) = \int_{-h}^{\eta(t)|_{x=l}} p\big|_{x=l}\,\mathrm{d}z - k(\xi(t) + \xi_0), \tag{30}$$

where m, k, p and $\eta(t)$ are mass of wall, constant of spring, pressure of fluid, and elevation of free surface, respectively, and $\xi_0 = \rho g h^2/2k$ is the pre-compression length of the spring against the static pressure of the liquid. According to the Bernoulli equation and using equation (14), we can obtain the following expression for the fluid pressure in the nth mode at the right wall boundary:

$$\begin{aligned} p\big|_{x=l} &= -\rho g z - \rho \frac{\partial \phi}{\partial t}\bigg|_{x=l} = -\rho g z - \rho\bigg[\frac{x^2 - (z+h)^2}{2l}\ddot{\xi}(t) \\ &\quad - \sum_{n=0}^{\infty} \frac{\beta_n}{\cosh k_n h} \cos k_n x \cosh k_n (z+h) \int_0^t \dddot{\xi}(\tau) \cos \omega_n (t-\tau)\,\mathrm{d}\tau\bigg]\bigg|_{x=l} \\ &= -\rho g z - \rho\bigg[\frac{l^2 - (z+h)^2}{2l}\ddot{\xi}(t) \\ &\quad - \frac{(-1)^n \beta_n}{\cosh k_n h} \cosh k_n (z+h) \int_0^t \dddot{\xi}(\tau) \cos \omega_n (t-\tau)\,\mathrm{d}\tau\bigg]. \end{aligned} \tag{31}$$

Then, by substituting equation (31) into (30), we can obtain the governing fluid-wall coupled equation in terms of $\xi(t)$ as follows:

$$(m+E)\ddot{\xi}(t) + k\xi(t) = F\int_0^t \dddot{\xi}(\tau) \cos \omega_n (t-\tau)\,\mathrm{d}\tau, \tag{32}$$

where E and F are constants given by

$$E = \rho \frac{lh}{2} - \rho \frac{h^3}{6l}, \qquad F = \frac{2\rho l^2}{(n\pi)^3} \tanh k_n h. \tag{33}$$

E comes from ϕ_F and works as a ''virtual mass'' in equation (32). The first term of E is equal to half of the fluid mass in the tank, so this term can be regarded as a ''fluid inertia''. The second term of E is related to the pressure change caused by the change of average water level. It has a minus sign because the change of water level always helps the spring to move the wall. F, on the other hand, comes from ϕ_1 and is related to the pressure change caused by the sloshing.

As equation (32) involves the convolution integral, and techniques of the conventional modal analysis are not applicable, we need the Laplace transform to solve it. Using Laplace transforms, we can obtain the following equation:

$$(m+E)[s^2\tilde{\xi}(s) - s\xi(0) - \dot{\xi}(0)] + k\tilde{\xi}(s) = F[s^3\tilde{\xi}(s) - s^2\xi(0) - s\dot{\xi}(0) - \ddot{\xi}(0)]\frac{s}{s^2 + \omega_n^2}, \tag{34}$$

where the tilde denotes a transformed quantity and s is the Laplace variable. Equation (34) can be rewritten in the form of transfer function as follows;

$$\tilde{\xi}(s) = \frac{\xi(0)s^3 + \dot{\xi}(0)s^2 + \dfrac{(m+E)\omega_n^2\xi(0) - F\ddot{\xi}(0)}{m+E-F}s + \dfrac{(m+E)\omega_n^2\dot{\xi}(0)}{m+E-F}}{s^4 + \dfrac{(m+E)\omega_n^2 + k}{m+E-F}s^2 + \dfrac{k\omega_n^2}{m+E-F}}$$

$$= \frac{\xi(0)s^3 + \dot{\xi}(0)s^2 + \dfrac{(m+E)\omega_n^2\xi(0) - F\ddot{\xi}(0)}{m+E-F}s + \dfrac{(m+E)\omega_n^2\dot{\xi}(0)}{m+E-F}}{(s^2+\omega_+^2)(s^2+\omega_-^2)}. \tag{35}$$

In this equation, ω_+ and ω_- are the two poles of the transfer function, and correspond to the frequencies of the fluid-wall coupled system. They are expressed as follows:

$$\omega_\pm^2 = \frac{[(1+E/m)\omega_n^2 + \omega_b^2] \pm \sqrt{[(1+E/m)\omega_n^2 + \omega_b^2]^2 - 4(1+E/m-F/m)\omega_n^2\omega_b^2}}{2(1+E/m-F/m)}, \tag{36}$$

where ω_n and ω_b are the natural frequency of sloshing in a rigid tank and that of the wall with no liquid ($\sqrt{k/m}$), respectively. Both ω_+ and ω_- are real, since the expression in square root in equation (36) is always non-negative. Therefore it is concluded that the fluid-wall coupled system has two natural frequencies for each sloshing mode. It should be pointed out that in equation (36) sloshing is in the nth mode, while the movement of wall does not belong to any category of a 'mode' because it is a rigid wall supported by a spring.

From equation (36) we can find the following order among ω_n, ω_+ and ω_-:

$$\omega_+ > \omega_n > \omega_-, \tag{37}$$

and the following limit for infinitely large k:

$$\lim_{k\to\infty} \omega_+ = \infty, \qquad \text{and} \quad \lim_{k\to\infty} \omega_- = \omega_n. \tag{38}$$

2.2.2. *Rotation case*

The equation of motion of the spring-supported wall in the rotation case is written as

$$I\ddot{\theta}(t) = \int_{-h}^{\eta(t)|_{x=l}} p\big|_{x=l}(h+z)\,\mathrm{d}z - kL^2(\theta(t)+\theta_0), \tag{39}$$

where I and L are the moment of inertia and length of the wall from the hinge to the spring, respectively; $\theta_0 = \rho g h^3/6kL^2$ is the pre-compression angle of the spring against the static pressure of the liquid. Similarly to the translation case, the governing fluid-wall coupled equation in terms of $\theta(t)$ of the right wall can be written as

$$(I+E)\ddot{\theta}(t) + kL^2\theta(t) = F\int_0^t \dddot{\theta}(\tau)\cos\omega_n(t-\tau)\,\mathrm{d}\tau, \tag{40}$$

where E and F are as follows [for details, please refer to appendix II.B in Lu (1995)]:

$$E = \rho\frac{lh^3}{8} - \rho\frac{h^5}{16l} + \frac{8\rho h^4}{\pi^5}\sum_{m=1}^{\infty}\frac{1}{(2m-1)^5\tanh[(2m-1)\pi l/h]} \tag{41}$$

and

$$F = \frac{2\rho l^2}{(n\pi)^3}\frac{h}{2}\left[1 + \frac{8}{\pi^2}\left(\sum_{m=1}^{\infty}\frac{1}{(2m-1)^2} - \sum_{m=1}^{\infty}\frac{1}{(2m-1)^2 + (nh/l)^2}\right)\right]$$
$$\times\left[h\tanh\frac{n\pi h}{l} - \frac{l}{n\pi}\left(1 - \frac{1}{\cosh[n\pi h/l]}\right)\right]. \quad (42)$$

E and F have similar physical meanings to those in the translation case, except for the terms expressing the rotational inertia. The third term of E is newly arisen and comes from ϕ_{Fr}. It is related to the pressure caused by the change of rotational flow velocity. The second term in the first bracket of F is related to the contribution of rotational flow to the sloshing. The value of the first bracket in F is nearly equal to unity for a shallow tank, and is nearly equal to 2 for a deep tank.

Using Laplace transforms, we can obtain two natural frequencies of the fluid-wall coupled system in the rotation case in terms of the natural frequency of sloshing ω_n and that of the right wall $\omega_b = \sqrt{kL^2/I}$; i.e.

$$\omega_{\pm}^2 = \frac{[(1+E/I)\omega_n^2 + \omega_b^2] \pm \sqrt{[(1+E/I)\omega_n^2 + \omega_b^2]^2 - 4(1+E/I-F/I)\omega_n^2\omega_b^2}}{2(1+E/I-F/I)}. \quad (43)$$

Relations similar to equations (37) and (38) also hold in the rotation case.

2.2.3. *Beat period*

Because of the existence of two natural frequencies, we can predict the occurrence of beats. If the sloshing is excited by setting the spring-supported wall out of the equilibrium position and then releasing it, we can set the initial conditions as follows:

$$\xi(0) \neq 0, \qquad \dot{\xi}(0) = 0 \quad \text{and} \quad \ddot{\xi}(0) \neq 0. \quad (44)$$

So we can rewrite equation (35) as follows:

$$\tilde{\xi}(s) = \frac{s\left[\xi(0)s^2 + \dfrac{(m+E)\omega_n^2\xi(0) - F\ddot{\xi}(0)}{m+E-F}\right]}{(s^2+\omega_+^2)(s^2+\omega_-^2)} = \frac{Qs}{s^2+\omega_+^2} + \frac{Rs}{s^2+\omega_-^2}, \quad (45)$$

where Q and R are constants given by

$$Q = \frac{-(m+E)\omega_n^2\xi(0) + (m+E-F)\omega_+^2\xi(0) + F\ddot{\xi}(0)}{(m+E-F)(\omega_+^2-\omega_-^2)}, \quad (46)$$

$$R = \frac{(m+E)\omega_n^2\xi(0) - (m+E-F)\omega_-^2\xi(0) - F\ddot{\xi}(0)}{(m+E-F)(\omega_+^2-\omega_-^2)}. \quad (47)$$

Performing the inverse Laplace transform on equation (45), we obtain

$$\xi(t) = Q\cos\omega_+ t + R\cos\omega_- t$$
$$= (Q+R)\cos\frac{\omega_+-\omega_-}{2}t\cos\frac{\omega_++\omega_-}{2}t + (Q-R)\sin\frac{\omega_+-\omega_-}{2}t\sin\frac{\omega_++\omega_-}{2}t. \quad (48)$$

Equation (48) indicates that if $Q \gg R$ or $Q \ll R$, the wall oscillates with almost the

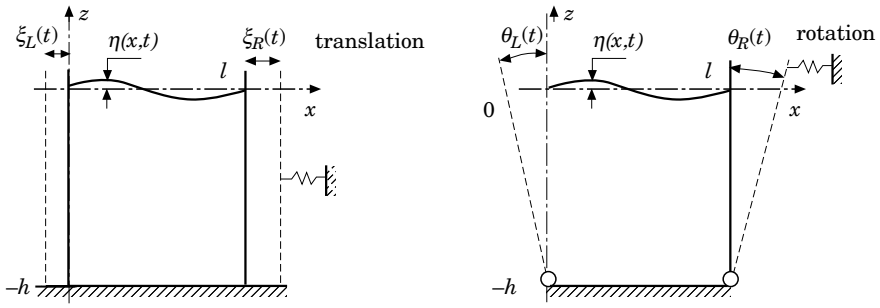

(a) Translation case (b) Rotation case

Figure 5. Fluid motion in a tank having two movable walls, showing two different types of wall motion.

natural frequency of ω_+ or ω_-; while the wall vibration displays the beating phenomenon if $Q \approx R$. In the latter case, the beat period is determined by

$$T = \frac{2\pi}{\omega_+ - \omega_-}. \tag{49}$$

2.3. Fluid-wall Interaction Excited by the Second Wall

We now solve the fluid-wall interaction in a tank having two movable walls as shown in Figure 5.

2.3.1. *Translation case*

We need to add to the flow velocity potential the terms for the left wall vibration. We rewrite ϕ in equation (14) as ϕ_R in this subsection, and obtain ϕ_L by a symmetry transformation of ϕ_R as follows:

$$\phi_L = -\frac{(x-l)^2 - (z+h)^2}{2l}\dot{\xi}_L(t) + \sum_{n=0}^{\infty} \frac{\beta_n}{\omega_n \cosh k_n h} \cos k_n(x-l) \cosh k_n(z+h) \int_0^t \dddot{\xi}_L(\tau) \sin \omega_n(t-\tau)\, \mathrm{d}\tau. \tag{50}$$

Thus, the total flow velocity potential in the tank having two movable walls can be written as

$$\phi = \phi_R + \phi_L. \tag{51}$$

By the same process as in Section 3.1.2, the governing fluid–wall coupled equation can be written as

$$(m+E)\ddot{\xi}_R(t) + k\xi_R(t) = F\int_0^t (\dddot{\xi}_R(\tau) - (-1)^n \dddot{\xi}_L(\tau)) \cos \omega_n(t-\tau)\, \mathrm{d}\tau - G\ddot{\xi}_L(t), \tag{52}$$

where the new coefficient $G = \rho \dfrac{h^3}{6l}$ is related to the pressure imposed on the right wall caused by the change of water level due to the movement of the left wall.

Firstly, we discuss the growth rate of the right wall vibration. We oscillate the left wall sinusoidally with the natural frequency ω_+ or ω_- as follows:

$$\dot{\xi}_L(t) = D \cos \omega_{\pm} t, \tag{53}$$

where D denotes the amplitude. By substituting equation (53) into (52) and using the Laplace transform, we obtain

$$(m+E)s^2\tilde{\xi}_R(s)+k\tilde{\xi}_R(s)=F\left[s^3\tilde{\xi}_R(s)+\frac{(-1)^nD\omega_\pm^2 s}{s^2+\omega_\pm^2}\right]\frac{s}{s^2+\omega_n^2}+\frac{GD\omega_\pm^2}{s^2+\omega_\pm^2}, \tag{54}$$

where the right wall is assumed at the equilibrium position in the beginning. Equation (54) can be rewritten in the form of a transfer function as follows:

$$\tilde{\xi}_R(s)=\frac{\dfrac{[(-1)^nF+G]D\omega_\pm^2 s^2+GD\omega_\pm^2\omega_n^2}{(m+E-F)(s^2+\omega_\pm^2)}}{(s^2+\omega_+^2)(s^2+\omega_-^2)}=\frac{1}{s^2+\omega_\pm^2}\left(\frac{A^\pm}{s^2+\omega_+^2}+\frac{B^\pm}{s^2+\omega_-^2}\right), \tag{55}$$

where $A^\pm$ and $B^\pm$ are constants given by

$$A^\pm=\frac{D\omega_\pm^2}{m+E-F}\frac{-G\omega_n^2+((-1)^nF+G)\omega_+^2}{\omega_+^2-\omega_-^2}, \tag{56}$$

$$B^\pm=\frac{D\omega_\pm^2}{m+E-F}\frac{G\omega_n^2-((-1)^nF+G)\omega_-^2}{\omega_+^2-\omega_-^2}. \tag{57}$$

Then performing the inverse Laplace transform on equation (55), we obtain the following form for the vibration of the right wall:

$$\xi_R^\pm(t)=\frac{A^\pm}{\omega_\pm\omega_+}\int_0^t \sin\omega_\pm\tau\sin\omega_+(t-\tau)\,\mathrm{d}\tau+\frac{B^\pm}{\omega_\pm\omega_-}\int_0^t \sin\omega_\pm\tau\sin\omega_-(t-\tau)\,\mathrm{d}\tau. \tag{58}$$

By integrating by parts, this equation can be rewritten as follows:

$$\begin{aligned}\xi_R^+(t)&=\frac{A^+}{\omega_+^2}\int_0^t \sin\omega_+\tau\sin\omega_+(t-\tau)\,\mathrm{d}\tau+\frac{B^+}{\omega_+\omega_-}\int_0^t \sin\omega_+\tau\sin\omega_-(t-\tau)\,\mathrm{d}\tau\\&=-\frac{A^+}{2\omega_+^2}t\cos\omega_+t+\frac{A^+}{\omega_+^3}\sin\omega_+t+\frac{B^+(\omega_+\sin\omega_-t-\omega_-\sin\omega_+t)}{\omega_+\omega_-(\omega_+^2-\omega_-^2)},\end{aligned} \tag{59}$$

and

$$\begin{aligned}\xi_R^-(t)&=\frac{B^-}{\omega_-^2}\int_0^t \sin\omega_-\tau\sin\omega_-(t-\tau)\,\mathrm{d}\tau+\frac{A^-}{\omega_+\omega_-}\int_0^t \sin\omega_-\tau\sin\omega_+(t-\tau)\,\mathrm{d}\tau\\&=-\frac{B^-}{2\omega_-^2}t\cos\omega_-t+\frac{B^-}{\omega_-^3}\sin\omega_-t+\frac{A^-(\omega_-\sin\omega_+t-\omega_+\sin\omega_-t)}{\omega_+\omega_-(\omega_-^2-\omega_+^2)}.\end{aligned} \tag{60}$$

The coefficients of the terms $t\cos\omega_\pm t$ are related to the growth rate. They are written, respectively, as

$$G_\xi^+=-\frac{A^+}{2\omega_+^2}\quad\text{and}\quad G_\xi^-=-\frac{B^-}{2\omega_-^2}. \tag{61}$$

Growth rates are the absolute values of $G_\xi^\pm$ in equation (61). Here we discuss the growth rate corresponding to ω_- as an example. Using equation (57) it is rewritten as follows:

$$\mathrm{GR}_\xi^-=\left|\frac{B^-}{2\omega_-^2}\right|=\left|\frac{D}{2(m+E-F)}\frac{G\omega_n^2-((-1)^nF+G)\omega_-^2}{\omega_+^2-\omega_-^2}\right|. \tag{62}$$

2.3.2. *Rotation case*

By a similar process, we can obtain the coefficient G in the rotation case as follows;

$$G = \rho \frac{h^5}{16l} - \frac{8\rho h^4}{\pi^5} \sum_{m=1}^{\infty} \frac{1}{(2m-1)^5 \sinh[(2m-1)\pi l/h]}. \tag{63}$$

The growth rate of wall vibration and the growth rate ratio of sloshing in the rotation case have the same form as those in the translation case, except that the mass m is replaced by the moment of inertia I, and the parameters such as E, F, G, $\omega_{\pm}$, β_n and so on are used in the rotation case.

2.4. Spring-mass Model

We finally simplify the fluid-wall coupled system into a simple spring-mass model when k is large enough to use the Taylor expansion.

First, we discuss ω_-. We rewrite ω_-^2 in equation (36) by taking its inverse, i.e.

$$\frac{1}{\omega_-^2} = \frac{[(1+E/m)\omega_n^2 + \omega_b^2] + \sqrt{[(1+E/m)\omega_n^2 + \omega_b^2]^2 - 4(1+E/m-F/m)\omega_n^2\omega_b^2}}{2\omega_n^2\omega_b^2}$$

$$= \frac{(1+E/m)\omega_n^2 + \omega_b^2}{\omega_n^2\omega_b^2} \frac{1}{2}\left[1 + \sqrt{1 - \frac{4(1+E/m-F/m)\omega_n^2\omega_b^2}{[(1+E/m)\omega_n^2 + \omega_b^2]^2}}\right]. \tag{64}$$

Then by applying the Taylor expansion to the square root term, we can rewrite equation (64) as follows:

$$\frac{1}{\omega_-^2} = \left(\frac{1+E/m}{\omega_b^2} + \frac{1}{\omega_n^2}\right)\left[1 - \frac{1}{4}\frac{4(1+E/m-F/m)\omega_n^2\omega_b^2}{[(1+E/m)\omega_n^2 + \omega_b^2]^2} - \frac{1}{16}\left\{\frac{4(1+E/m-F/m)\omega_n^2\omega_b^2}{[(1+E/m)\omega_n^2 + \omega_b^2]^2}\right\}^2 + \dots\right]. \tag{65}$$

If k is very large, we can simplify equation (65) into the following form:

$$\frac{1}{\omega_-^2} \approx \frac{1+E/m}{\omega_b^2} + \frac{1}{\omega_n^2} = \frac{1}{\omega_b'^2} + \frac{1}{\omega_n^2}, \tag{66}$$

where $\omega_b' = \sqrt{k/(m+E)}$ is the natural vibration frequency of the wall of the tank containing non-sloshing liquid. For the rotation case, we use $\omega_b' = \sqrt{kL^2/(I+E)}$ in the above derivation.

Second, we discuss ω_+. By applying the Taylor expansion here also, we can rewrite ω_+^2 in equation (36) as follows:

$$\omega_+^2 = \frac{(1+E/m)\omega_n^2 + \omega_b^2}{1+E/m-F/m} \frac{1}{2}\left[1 + \sqrt{1 - \frac{4(1+E/m-F/m)\omega_n^2\omega_b^2}{[(1+E/m)\omega_n^2 + \omega_b^2]^2}}\right]$$

$$= \frac{(1+E/m)\omega_n^2 + \omega_b^2}{1+E/m-F/m}\left[1 - \frac{1}{4}\frac{4(1+E/m-F/m)\omega_n^2\omega_b^2}{[(1+E/m)\omega_n^2 + \omega_b^2]^2} - \frac{1}{16}\left\{\frac{4(1+E/m-F/m)\omega_n^2\omega_b^2}{[(1+E/m)\omega_n^2 + \omega_b^2]^2}\right\}^2 + \dots\right]$$

$$\approx \omega_n^2 + \frac{\omega_b^2}{1+E/m} = \omega_n^2 + \omega_b'^2. \tag{67}$$

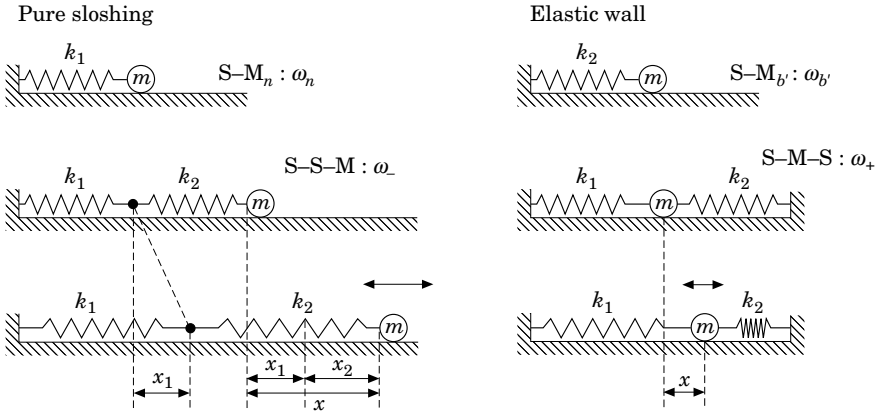

Figure 6. The types of wall motion. Spring-mass model.

Equations (66) and (67) can be elucidated by means of a spring-mass model. First, we represent sloshing in a rigid tank and wall vibration without sloshing by S-M$_n$ and S-M$_{b'}$, respectively, in Figure 6. The natural frequencies of S-M$_n$ and S-M$_{b'}$ are related to the mass and spring stiffness as follows:

$$\omega_n^2 = \frac{k_1}{m} \quad \text{and} \quad \omega_b'^2 = \frac{k_2}{m}. \tag{68}$$

Then equation (66) for ω_- can be represented by the S-S-M model in Figure 6, since the following relation holds:

$$\omega_{\mathrm{SSM}}^2 = \frac{k_1 k_2}{m(k_1 + k_2)} = \frac{1}{\dfrac{1}{\omega_n^2} + \dfrac{1}{\omega_b'^2}} = \omega_-^2 . \tag{69}$$

In the same manner, equation (67) for ω_+ can be represented by the S-M-S model, since

$$\omega_{\mathrm{SMS}}^2 = \frac{k_1 + k_2}{m} = \omega_n^2 + \omega_b'^2 = \omega_+^2. \tag{70}$$

Although the present system is illustrated by a spring-mass model, the manner of connection in the present model is different from those seen in the conventional modal analysis because the springs are connected in series in the S-S-M model, while a single mass is connected to the walls by two springs in the S-M-S model.

3. VALIDATION OF THEORETICAL METHOD

A numerical method was also developed to analyse the fluid-wall interaction (Lu *et al.* 1995a). This numerical method was established on the basis of the PCBFC (Physical Component Boundary Fitted Coordinate) method (Takizawa *et al.* 1992; Takizawa & Kondo 1993). The PCBFC method has good numerical accuracy and stability because

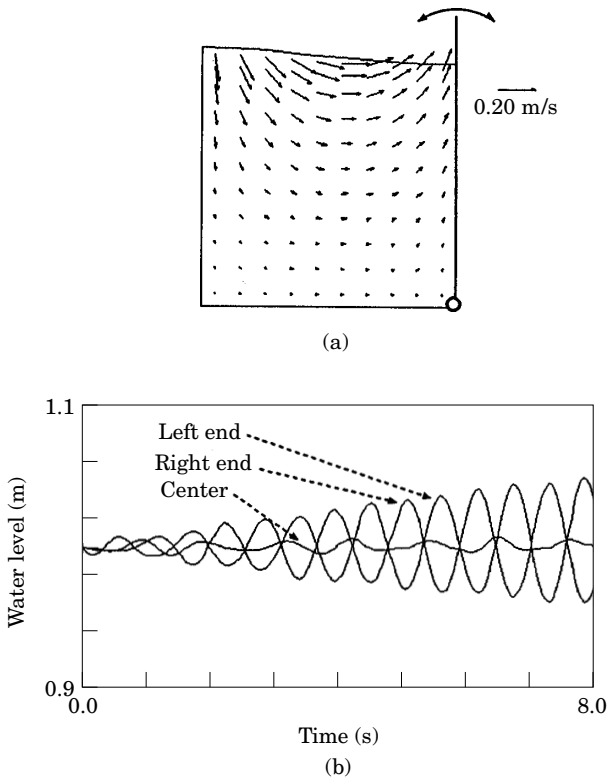

Figure 7. Resonant sloshing induced by wall oscillation (rotation case): (a) flow pattern at $t = 8$ s; (b) time history of water level.

it is a kind of BFC method using the physical components (PC) as variables and a physical curvilinear space as the analytical space. In the present section we shall discuss the agreement between the analytical results and the numerical ones.

3.1. Sloshing Excited by a Movable Wall

Corresponding to Section 2.1.3, Lu *et al.* (1995a) numerically generated the resonant sloshing with a first-mode wave in a 1m × 1m water tank [illustrated in Figure 7(a)] by rotating the right wall with the following function:

$$\dot{\theta}(t) = D \cos \omega_1 t = 0{\cdot}005 \times 5{\cdot}54 \cos 5{\cdot}54t. \tag{71}$$

As shown in Figure 7(b), the water level at the right end reaches a peak at the time of about 7·3 s. Therefore the growth rate of sloshing was estimated to be

$$\mathrm{GR} = \frac{1{\cdot}045 - 1{\cdot}0000}{7{\cdot}3} = 0{\cdot}00616 \text{ m/s}. \tag{72}$$

Substituting equation (23) into equation (29), the analytical growth rate of sloshing was estimated to be

$$\mathrm{GR} = \frac{D\omega_1^2}{2g}\frac{1}{\pi^2}\left[2 - \frac{4}{\pi}\left(\frac{\mathrm{e}^{\pi}}{\sinh \pi} - \frac{\mathrm{e}^{\pi/2}}{2\sinh\dfrac{\pi}{2}} - \frac{1}{2}\right)\right] = 0{\cdot}00622 \text{ m/s}. \tag{73}$$

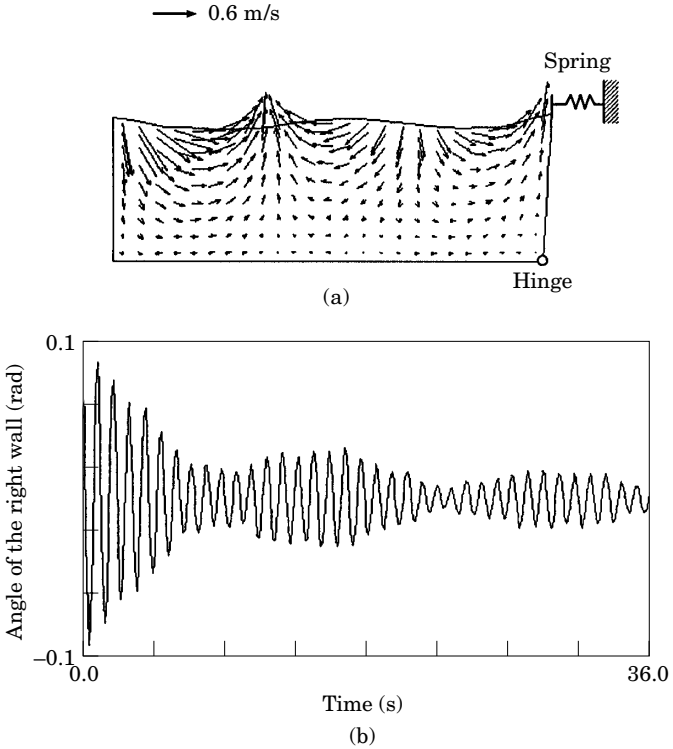

Figure 8. Fluid-wall interaction in a tank having spring-supported wall: (a) flow pattern at $t = 4$ s; (b) time history of right-wall angle.

Thus, the growth rate obtained numerically is well predicted by the present analytical model.

3.2. Beat Phenomenon

Corresponding to Section 2.2.3, Lu *et al.* (1995a) chose the following geometry and parameters for the numerical analysis, the same as Eguchi *et al.* (1990);

$$l = 2{\cdot}5\ \text{m}, \qquad h = 0{\cdot}8\ \text{m}, \qquad L = 1{\cdot}0\ \text{m}, \qquad I = 1 \times 10^3\ \text{kg m}^2, \quad \text{and} \quad k = 4 \times 10^4\ \text{N/m}.$$

The sloshing is initiated by putting the rotatable right wall out of the equilibrium position and then releasing it. As shown in Figure 8(a), the sloshing is in the third mode. So we can estimate E, F and ω_3 as follows:

$$E = 0{\cdot}1625 \times 10^3, \qquad F = 0{\cdot}0065 \times 10^3 \quad \text{and} \quad \omega_3 = 6{\cdot}064\ \text{Hz}.$$

Then, using equation (49) we can estimate the theoretical period of beats as follows;

$$T = \frac{2\pi}{\sqrt{38{\cdot}57} - \sqrt{33{\cdot}01}} = 13{\cdot}5\ \text{s}. \tag{74}$$

As shown in Figure 8(b), a beat phenomenon is observed in the wall vibration. The numerically computed period of the beats is measured to be

$$T = 23{\cdot}0 - 9{\cdot}7 = 13{\cdot}3\ \text{s}, \tag{75}$$

which is in good agreement with the analytical prediction.

3.3. Fluid-wall Interaction Excited by the Second Wall

Corresponding to Section 2.3, we first confirm that there are two natural frequencies in the fluid–wall coupled system. We chose a 2-D tank with a spring-supported rotatable right wall, as illustrated in Figure 5(b), with the following geometry:

$$l = 1{\cdot}0\,\text{m}, \qquad h = 1{\cdot}0\,\text{m}, \qquad L = 1{\cdot}0\,\text{m},$$

and the following parameters:

$$k = 10\,000{\cdot}0\,\text{N/m} \quad \text{and} \quad I = 300\,\text{kg m}^2.$$

The geometry was chosen for simplicity and the parameters make the natural frequency of the rotatable wall comparable to the natural frequency of sloshing. Using the formulae obtained in Section 2, we estimate E, F, G, ω_n, ω_b, ω_+ and ω_- as follows:

$$E = 88{\cdot}85, \qquad F = 32{\cdot}22, \qquad G = 60{\cdot}24,$$

$$\omega_1 = 5{\cdot}538\,\text{Hz}, \qquad \omega_b = 5{\cdot}774\,\text{Hz}, \qquad \omega_+ = 6{\cdot}321\,\text{Hz}, \qquad \omega_- = 4{\cdot}639\,\text{Hz}.$$

Then we oscillate the left wall with angular velocities $\dot{\theta}_L^+$ and $\dot{\theta}_L^-$, respectively:

$$\dot{\theta}_L^{\pm}(t) = 0{\cdot}1 \cos \omega_{\pm} t. \tag{76}$$

The numerical results are shown in Figure 9. Both the frequencies of the sloshing and the wall vibration are equal to ω_+ in Figure 9(a), and equal to ω_- in Figure 9(b). The vibration amplitudes of the wall and water level increase with time almost linearly in these two cases, indicating that both ω_+ and ω_- are natural frequencies of the coupled system.

Secondly, we also predicted the growth rate of the wall vibration. Take the case having natural frequency ω_- as an example. The growth rate of the wall vibration

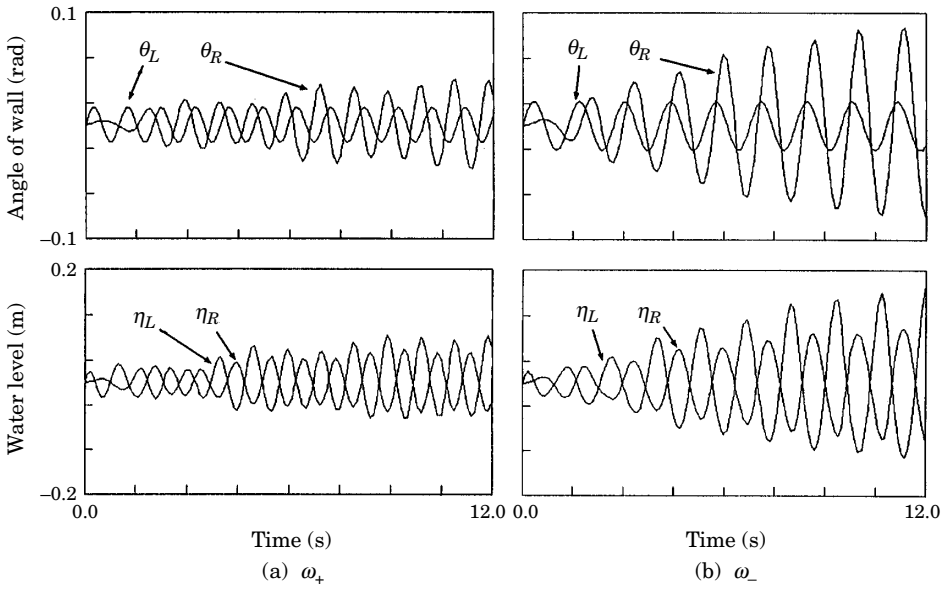

Figure 9. Time histories of sloshing and vibration of the walls in a two-movable-wall tank.

estimated from Figure 9(b) is 0·008 rad/s. The growth rate of wall vibration predicted by equation (62) is 0·009 rad/s. In the same way, we also found in the case having natural frequency ω_+ that the growth rates are accurately predicted by the present theory.

4. ANALYSIS OF OVERFLOW-INDUCED VIBRATION OF THE WEIR

4.1. Theoretical Analysis

4.1.1. *Velocity potential related to the overflow*

We have done the numerical investigation first. It was found by numerical computation (Lu *et al.* 1995b) that the oscillatory part of the overflow is the motive force for the growth of the weir vibration. Then we carried out numerical computation by ignoring the constant part from the overflow as illustrated in Figure 10(a). In this case the vortex flow in the downstream tank never appears, as shown in Figure 10(b), and hence in this case the flow in the downstream tank can be considered as a potential flow. Therefore we can derive the governing equation for this potential flow by modifying

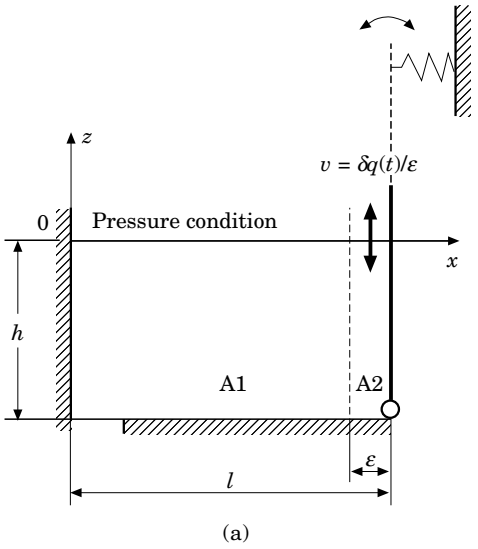

(a)

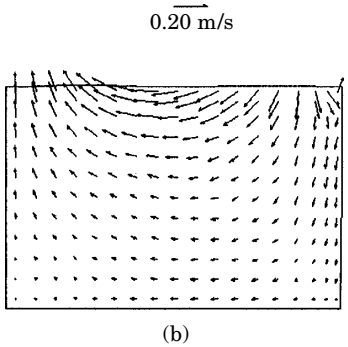

(b)

Figure 10. Physical model of overflow: (a) schematic for the analysis of the overflow; (b) computed flow pattern at $t = 8$ s.

the boundary condition at the weir and that at the free surface in equations (1)–(4) as follows:

$$\left.\frac{\partial \phi}{\partial x}\right|_{x=l} = (z+h)\dot{\theta}_R(t), \tag{77}$$

$$\left.\frac{\partial \phi}{\partial z}\right|_{z=0} = \begin{cases} \dfrac{-1}{g}\left.\dfrac{\partial^2 \phi}{\partial t^2}\right|_{z=0}; & 0 \le x \le l-\varepsilon \\ \dfrac{\delta q(t-\tau)}{\varepsilon}; & l-\varepsilon \le x \le l \end{cases} \tag{78}$$

where $\delta q(t-\tau)$ and ε are the oscillatory part of the overflow and the width of inlet, respectively, and τ denotes the time delay experienced by the overflow from the time of leaving the top of the weir to arriving at the free surface of the downstream tank.

Since it is difficult to solve the potential flow equation with the boundary conditions written above, we have modified these boundary conditions. We separate the downstream tank into two regions: A1 and A2, as shown in Figure 10(a). A2 is a strip region just below the injection of overflow. Since A2 is very narrow, we can neglect this region and take it as just giving the horizontal velocity distribution at the right side of A1. In order to obtain the velocity distribution we have performed a numerical computation of the flow in the downstream tank for a short time, such as 0·2 s, shorter than the natural period of the weir vibration, as illustrated in Figure 11(a), where the weir is fixed and the top boundary is also fixed, and both the inlet and outlet velocity are 0·767 m/s. Figure 11(b) illustrates the computed velocity distribution at 0·2 s at the interface between A1 and A2. So we can model the velocity distribution in Figure 11(b) as that of the rotation flow illustrated in Figure 11(c). Then, we can assume that the oscillatory part of the overflow in Figure 10(a) gives an oscillatory rotation velocity distribution near the weir. Therefore the oscillatory part of the overflow looks like a

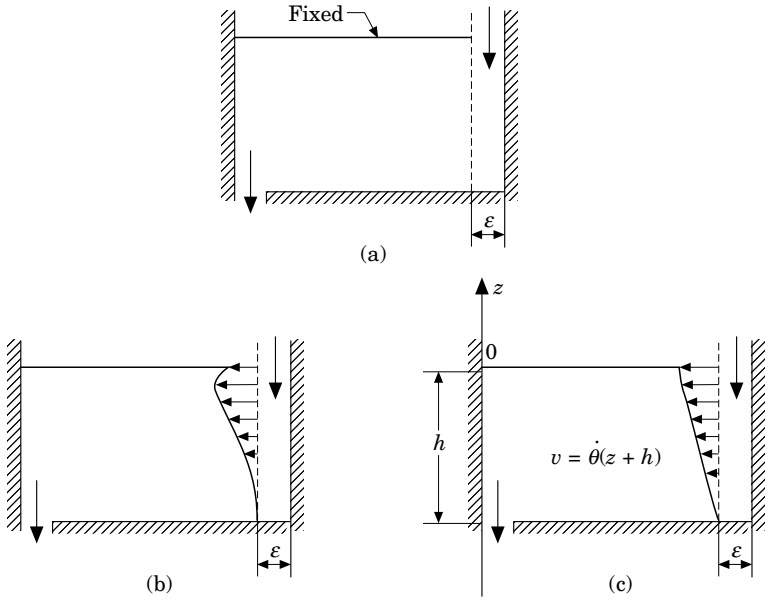

Figure 11. Velocity distribution: (a) the system for which the computation was conducted (with equal inlet and outlet velocities); (b) the computed velocity distribution at 0·2 s; (c) the flow distribution in the rotation flow case.

virtual oscillatory wall. Using this assumption, the present system can be treated as a kind of fluid–wall coupled system having two movable walls as shown in Figure 5, the only difference being that the two movable walls are situated at the same side of the tank. The angular velocity of the horizontal flow relative to the weir (or the angular velocity of the virtual oscillatory wall) can be estimated by the flow-rate conservation of region A2 as

$$\dot{\theta}(t) = \frac{2\delta q(t-\tau)}{h^2}. \tag{79}$$

Finally we can modify the boundary conditions in equations (77) and (78) as follows:

$$\left.\frac{\partial \phi}{\partial x}\right|_{x=l} = (z+h)[\dot{\theta}_R(t) - \dot{\theta}(t)], \tag{80}$$

$$\left.\frac{\partial \phi}{\partial z}\right|_{z=0} = -\frac{1}{g}\left.\frac{\partial^2 \phi}{\partial t^2}\right|_{z=0}. \tag{81}$$

Then by following the theoretical derivation of equation (52) in Section 2.3, we can obtain the governing fluid-weir coupled equation as

$$(I+E)\ddot{\theta}_R(t) + k\theta_R(t) = F\int_0^t (\ddot{\theta}_R(\tau) - \ddot{\theta}(\tau)) \cos \omega_n(t-\tau)\, \mathrm{d}\tau + E\ddot{\theta}(t), \tag{82}$$

where $\theta_R(t)$ is the angle of the weir, and the expressions of coefficients E and F are the same as in equations (41) and (42).

4.1.2. *Overflow rate in the upstream tank*

The overflow rate is estimated by the following empirical formula (Henderson 1966):

$$q(t) = \tfrac{2}{3} C_d \sqrt{2g}\, h^{3/2}(t), \tag{83}$$

where C_d and $h(t)$ denote an experimental coefficient and the thickness of overflow at the top of the weir, respectively, and $C_d = 0{\cdot}611$ is recommended. $h(t)$ in the above equation is solved by discretizing the following mass conservation equation in the upstream tank:

$$W\dot{h}(t) + q(t) - \tfrac{1}{2}H^2\dot{\theta}(t) = VW, \tag{84}$$

where H, W and V denote height, width of inlet and inlet velocity of the upstream tank, respectively. We separate the overflow rate into two parts as follows:

$$q(t) = q_0 + \delta q(t), \tag{85}$$

where q_0 is the inlet flow rate of the upstream tank. We then linearize the empirical equation (83),

$$q(t) = C_d\sqrt{2gh_0}h(t) = c_0 h(t), \tag{86}$$

where h_0 is the overflow height in the case that the weir is fixed, and can be determined by

$$q_0 = C_0 h_0. \tag{87}$$

Hence, C_0 is given by

$$C_0 = C_d\sqrt{2gh_0} = (2gC_d^2 q_0)^{1/3}. \tag{88}$$

By substituting equations (85) and (86) into (84), we can obtain

$$\frac{W}{C_0}\dot{\delta}q(t) + \delta q(t) = \tfrac{1}{2}H^2\dot{\theta}_R(t). \tag{89}$$

Equations (79), (82) and (89) form a homogeneous equation set.

4.1.3. *Characteristics of the overflow-induced vibration*

We next solve the aforementioned equation set. We can employ strict mathematics to show the exponential growth rate of the weir vibration. We begin the derivation by assuming $\theta_R(t)$ to grow exponentially [for explanation, please refer to appendix III.A in Lu (1995)]

$$\theta_R(t) = B\mathrm{e}^{at} \sin \omega_- t, \tag{90}$$

where B and a are unknown coefficients. Substituting equation (90) into equation (89), we obtain the overflow as follows:

$$\delta q(t) = R_0 B\mathrm{e}^{at} \sin \omega_-(t + \tau'), \tag{91}$$

where

$$R_0 = \tfrac{1}{2}H^2 \sqrt{\frac{a^2 + w_-^2}{(1 + Wa/C_0)^2 + (W\omega_-/C_0)^2}}, \tag{92}$$

and

$$\tau' = \frac{1}{\omega_-} \arctan \frac{\omega_-\left(1 + \dfrac{Wa}{C_0}\right) - a\left(\dfrac{W\omega_-}{C_0}\right)}{a\left(1 + \dfrac{Wa}{C_0}\right) + \omega_-\left(\dfrac{W\omega_-}{C_0}\right)}. \tag{93}$$

Since $a \ll \omega_-$, we can rewrite R_0 and τ'

$$R_0 = \frac{\tfrac{1}{2}H^2\omega_-}{\sqrt{1 + (W\omega_-/C_0)^2}}, \qquad \text{and} \quad \tau' = \frac{1}{\omega_-} \arctan \frac{C_0}{W\omega_-}. \tag{94}$$

Comparing equation (91) with equation (90), we see that the overflow at the top of the weir is always ahead of the weir vibration by the time τ'. If the time delay τ is equal to τ', the overflow at the free surface of the downstream tank is written as

$$\delta q(t - \tau) = R_0\mathrm{e}^{-a\tau} B\mathrm{e}^{at} \sin \omega_- t. \tag{95}$$

By substituting equation (95) into (79), we obtain the angular velocity of the virtual wall,

$$\dot{\theta}(t) = R\mathrm{e}^{-a\tau} B\mathrm{e}^{at} \sin \omega_- t, \tag{96}$$

where $R = 2R_0/h^2$. Then substituting equation (96) into (82), we finally obtain $\theta_R(t)$ as follows [for detailed derivation, please refer to appendix III.B in Lu (1995)]:

$$\theta_R(t) = R\mathrm{e}^{-a\tau} B \frac{X}{2a} \mathrm{e}^{at} \sin \omega_- t, \tag{97}$$

where X is given by

$$X = \frac{E(\omega_n^2 - \omega_-^2) + F(a^2 + \omega_-^2)}{(I + E - F)(\omega_+^2 - \omega_-^2)}. \tag{98}$$

Comparing equations (97) and (90), we obtain the following equality:

$$R\mathrm{e}^{-a\tau} B \frac{X}{2a} = B, \tag{99}$$

and therefore obtain the exponential growth rate as follows:

$$a = \tfrac{1}{2}R\mathrm{e}^{-a\tau} X = \tfrac{1}{2}R\mathrm{e}^{-a\tau} \frac{E(\omega_n^2 - \omega_-^2) + F(a^2 + \omega_-^2)}{(I + E - F)(\omega_+^2 - \omega_-^2)}. \tag{100}$$

Since $a \ll \omega_-$ and $e^{-a\tau} \approx 1$, equation (100) is simplified to

$$a = \frac{R}{2(I+E-F)} \cdot \frac{E(\omega_n^2 - \omega_-^2) + F\omega_-^2}{\omega_+^2 - \omega_-^2}, \tag{101}$$

where

$$R = 2\frac{R_0}{h^2} = \frac{H^2\omega_-}{h^2\sqrt{1+\left(\dfrac{W\omega_-}{C_0}\right)^2}} = \frac{H^2\omega_-}{h^2\sqrt{1+\left(\dfrac{W\omega_-}{(2gC_d^2q_0)^{1/3}}\right)^2}}.$$

a in equation (101) is always positive because $\omega_n > \omega_-$ and $\omega_+ > \omega_-$ [see equation (37)]. Because $\tau = \tau'$ is assumed in deriving equation (101) and under this condition the overflow and the weir vibration are always in phase, a in this case is the maximum growth rate. If we do not assume $\tau = \tau'$, the growth rate in equation (101) may be generalized as follows:

$$a(\tau) = a\cos\omega_-(\tau - \tau'), \tag{102}$$

i.e. as a sinusoidal function.

Comparing equation (101) with (62), it is clear that the theoretical results in this section are essentially the extensions of those in Section 2: the coefficient G in equation (62) is replaced by the term E in equation (101) because the overflow is dropped in the same side of the spring-supported weir; the term D in equation (62) is replaced by the term R in equation (101) because the amplitude of the virtual wall is also determined by the flow in the upstream tank.

In equation (101) a indicates the effect of elasticity of the weir on the growth rate. We can analyze a as follows. By substituting equation (43) into a, we obtain

$$a = R\frac{[E(1+E/I-2F/I)+F(1+E/I)]\omega_n^2 - (E-F)\omega_b^2}{4(I+E-F)\sqrt{[(1+E/I)\omega_n^2-\omega_b^2]^2 + 4F/I\omega_n^2\omega_b^2}} + R\frac{E-F}{4(I+E-F)}. \tag{103}$$

Then, by solving the differential equation

$$\frac{da}{d\omega_b} = \frac{d}{d\omega_b}\left[\frac{-R(E-F)}{4(I+E-F)} \cdot \frac{\omega_b^2}{\sqrt{[(1+E/I)\omega_n^2-\omega_b^2]^2 + 4F/I\omega_n^2\omega_b^2}}\right] = 0, \tag{104}$$

we can obtain the following condition:

$$(1+E/I-2F/I)\omega_b^2 = (1+E/I)^2\omega_n^2. \tag{105}$$

By substituting equation (105) into equation (103), we can obtain the following expression for a;

$$a = \frac{R}{4}\left(\frac{I-E}{I+E}\sqrt{\frac{F}{I+E-F}} + \frac{E-F}{I+E-F}\right). \tag{106}$$

When $I \gg E$ and $I \gg F$, equations (105) and (106) reduce to

$$\omega_b^2 = \omega_n^2, \qquad \text{and} \quad a_{\max} = \frac{R}{4}\left(\frac{E}{I} + \sqrt{\frac{F}{I}}\right). \tag{107,108}$$

Equations (107) and (108) indicate that a has a peak when $\omega_b^2 = \omega_n^2$. We can see from (108) that the peak height decreases with an increase of I. Therefore, the exponential growth rate of the weir has a peak value related to the elasticity of the weir. It is concluded that under the condition $\omega_b^2 = \omega_n^2$, the coupled system is synchronized such that it can absorb the most energy.

4.2. Validation of the Theoretical Results

The PCBFC method was further developed by Lu *et al.* (1995b) to simulate the overflow-induced vibration experiment performed by Fukuie & Hara (1989). In that simulation, the downstream tank is taken as the computational domain, and the upstream tank is taken into consideration by solving the flow rate balance equation in the upstream tank.

By taking advantage of the numerical method, we analysed the effect of time delay. The time delay as well as the injection velocity of the overflow at the inlet of the downstream tank are determined by the fall height ΔH (see Figure 2). However, we change the delay time τ artificially to single out its effect on the weir vibration, while the injection velocity of the overflow is fixed. The computed growth rate of the weir vibration in terms of the time delay τ (expressed in terms of the period T) is shown in Figure 12. From this figure we see that the overflow may either make the weir vibration amplitude grow or decay depending on the delay time. Two points are outstanding in this figure. First, the growth rate dependency is similar in shape to a sinusoidal function, although the peak is sharper and the trough is wider. Secondly, the peak has a delay time of approximately $T/10$.

Substituting equation (88) into equation (94), we estimate τ' as follows:

$$\tau' = \frac{1}{\omega_-} \arctan \frac{(2gC_d^2 q_0)^{1/3}}{W\omega_-} = \frac{T}{2\pi} \arctan \frac{(2 \times 9{\cdot}8 \times 0{\cdot}611^2 \times 0{\cdot}011)^{1/3}}{0{\cdot}1 \times (0{\cdot}82/2\pi)} \approx 0{\cdot}1T. \quad (109)$$

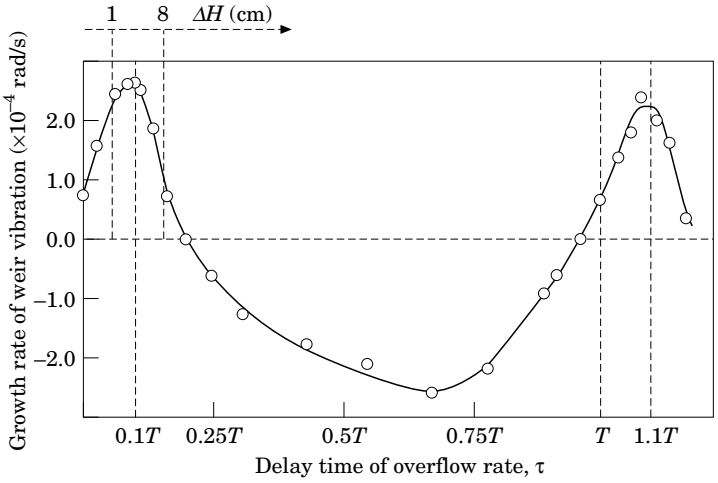

Figure 12. Effect of delay time on overflow-induced vibration; T is the period of sloshing ($T = 0{\cdot}82$ s).

Therefore, we can see that equation (102) predicts satisfactorily the positive peaks at $\tau \approx 0{\cdot}1T$ and $1{\cdot}1T$ and the negative valley near $\tau \approx 0{\cdot}6T$ in Figure 12.

Then we studied the dependence of the growth rate on the stiffness of the spring (k) and the inertia of the weir (I). In this case, we chose the inlet flow rate and fall height as follows:

$$q_0 = 0{\cdot}05 \text{ m/s} \times 0{\cdot}1 \text{ m}, \qquad \text{and} \quad \Delta H = 0{\cdot}01 \text{ m}.$$

We chose small q_0 and ΔH this time, to avoid the nonlinear effect which may invalidate the comparison between the numerical results and the analytical prediction. Theoretical and numerical exponential growth rates of the weir vibration are compared in Figure 13. As indicated in this figure, there is a peak in the growth rate for each weir inertia I, and the height of peak decreases with increasing stiffness k. The agreement is very good; especially the location of the peak is well predicted.

We also estimated the natural frequency of the weir ω_b corresponding to the peak in this figure, and find that it is very close to the natural frequency of pure sloshing ω_n. By comparison, we can see that the analytical derivation in the previous subsection is in good agreement with the present numerical analysis.

4.3. Limits of the Analytical Method

Using the numerical method, we also investigated the effect of the constant part of the overflow rate q_0 on the weir vibration. Since the constant part of the overflow is equal to the circulation flow rate of the loop, we performed computations by fixing the fall height at $\Delta H = 3$ cm, and changing the inlet flow rate from 3 to 23 cm/s. The numerical results are shown in Figure 14. The average velocity of the free surface flow in the downstream tank U increases with increasing circulation flow rate. With an increase of U, the growth rate of the weir vibration decreases and becomes negative after a peak. The growth rate in Figure 14 is predicted to be proportional to the

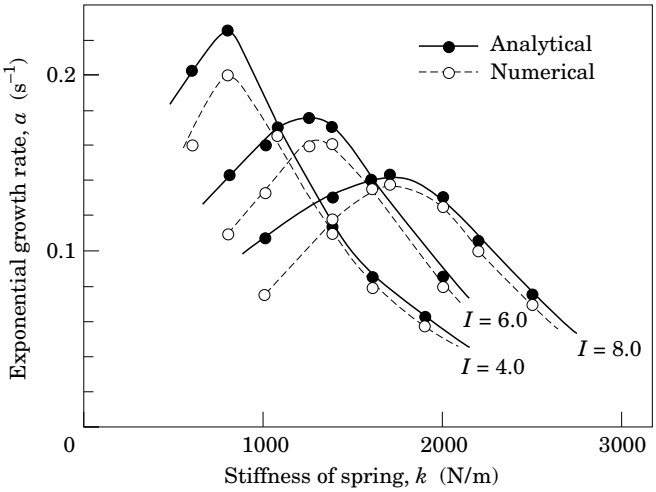

Figure 13. Exponential growth rate for an inlet flow rate of 5 cm/s and a fall height of 1 cm; the lines are lines of best fit through the computed points.

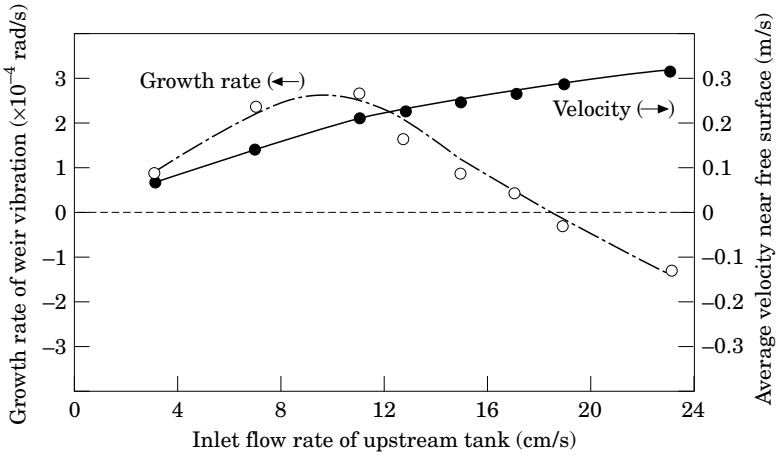

Figure 14. Effect of inlet flow rate q_0 on overflow-induced vibration for a fall height of 3 cm; the lines are lines of best fit through the computed points.

circulation flow rate if only the linear effects are considered. However, it has been shown by Takizawa & Kondo (1993) that U is proportional to the "sloshing Froude number (Frs)." When Frs exceeds a threshold value ($Frs_c = 0{\cdot}30 \sim 0{\cdot}35$), an effect called "flow-caused damping" is produced. In Figure 14, Frs exceeds this critical value when the inlet flow velocity of the upstream tank is larger than 15 cm/s. Therefore we can conclude that the "flow-caused damping" effect suppresses the sloshing, and subsequently suppresses the weir vibration when the inlet flow velocity of the upstream tank is larger than 15 cm/s. This is a nonlinear effect, which can only be found when we consider the effect of the constant part of overflow and is outside the capability of the present analytical approach.

5. CONCLUSIONS

A method different from a conventional modal analysis was developed for the analysis of the vibration of a wall coupled with the sloshing of fluid in a vessel. Since the governing equation of flow in the present case has nonhomogeneous Neumann boundary conditions, and the motion equation of the wall coupled with the sloshing has a convolution integral and high-order derivatives, the present formulation is beyond the scope of conventional modal analysis. Therefore, it was solved by the potential separation technique and the use of Laplace transforms. It is new in the sense that it is an extension of the method proposed by Aslam *et al.* (1979) and Fujita *et al.* (1985) and is applied to the coupled weir-sloshing problem.

By the present method, we succeeded in obtaining the explicit physical characteristics of fluid-wall interaction such as frequency, beat period, phase and growth rate, and also in giving a physical meaning to the present analytical results by means of a simplified spring-mass model. All these results help us to understand the detailed physical behavior of the fluid-wall interaction, and also supply benchmark results for numerical analysis in this field.

The analytical results obtained by the present method were shown to be in good agreement with those obtained by numerical analysis. Validation of the present method was confirmed.

An overflow model was proposed, in which the overflow acts as an oscillatory virtual

wall to give an oscillatory and rotatable velocity distribution in the downstream tank. Because it is established on the basis of a numerical analysis, it is more realistic than the pressure boundary assumption used previously. In addition, this model permits simplification of the mathematics required for analysis.

By comparing the resonant vibration in the two-movable-wall tank with the overflow-induced vibration, we can understand that the virtual oscillatory wall works as a vibration source and contributes to the growth of the overflow-induced vibration, just like the left wall in the two-movable-wall tank. This is one part of the mechanism of the vibration of the weir.

It was found that the weir vibration can be suppressed by selecting a moderate overflow height, since the overflow height determines the time required for the flow leaving the weir to reach the tank. It was also shown that the weir vibration can be alleviated by selecting a moderate stiffness and moment of inertia of the weir, so that the natural frequency of the weir mismatches the natural frequency of sloshing.

Validation of the present analytical model of the overflow-induced vibration of the weir was also demonstrated by comparison with numerical analysis. In addition, the nonlinear effect of the flow was discovered by the numerical analysis. For the first time, it was found that a so-called ''flow-caused damping'' effect may suppress the overflow-induced vibration. This is another mechanism of the vibration.

References

Aslam, M., Godden, W. G. & Scalise, D. T. 1979 Earthquake sloshing in annular and cylindrical tanks. *ASCE Journal of the Engineering Mechanics Division* **105,** 371–389.

Aïta, S., Tigeot, Y., Bertaut, C. & Serpantie, J. P. 1986 Fluidelastic instability of a flexible weir: experimental observations. In *Flow-Induced Vibration—1986* (eds S. S. Chen, J. C. Simonis & Y. S. Shin) PVP Vol. 104, pp. 41–50. New York: ASME.

Eguchi, Y. & Tanaka, N. 1990 Fluid-elastic vibration of flexible overflow weir. *JSME International Journal,* Series III **33,** 323–329.

Eguchi, Y. & Tanaka, N. & Koga, T. 1990 Simulation of thermal and dynamic fluid-structure interaction in a fast breeder reactor. In *Proceedings of the First International Conference on Supercomputing in Nuclear Applications,* pp. 86–91, Mito, Japan.

Fujita, K., Ito, T. & Okada, K. 1985 Seismic response of liquid sloshing in the annular region formed by coaxial circular cylinders. *Engineering Computations* **2,** 299–306.

Fujita, K., Ito, T., Kodama, T., Tanaka, N., Koga, T. & Eguchi, Y. 1992 Experimental study on flow-induced vibration of flexible weir due to fluid discharge. In *Fluid-Structure Vibration and Sloshing* (eds D. C. Ma, K. Fujita & J. Tani) PVP Vol. 232, pp. 71–76. New York: ASME.

Fujita, K., Ito, T., Kodama, T., Adachi, S., Sekine, K., Ozaki, H., Eguchi, Y. & Yamamoto, K. 1993 Study on flow-induced vibration of a flexible weir due to fluid discharge: effect of weir stiffness. In *Flow-Induced Vibration and Fluid-Structure Interaction—1993* (eds M. K. Au-Yang) PVP Vol. 258, pp. 143–150. See also *Journal of Fluids and Structures* **10,** 79–98 (1996).

Fukuie, M. & Hara, F. 1989 Experimental study of self-excited vibrations of a flexible weir due to flow discharge. *Transactions of JSME* **55,** No. 517, 2282–2289.

Hara, F. & Suziki, T. 1992 Dynamical instability analysis of self-excited vibration of a flexible weir due to fluid discharge. In *International Symposium on Flow-Induced Vibration and Noise–1992* (eds M. P. Paidoussis & M. K. Au-Yang) PVP Vol. 244, pp. 45–58. New York: ASME.

Henderson, F. M. 1966 *Open Channel Flow.* New York: Macmillan.

Kaneko, S., Watanabe, T. & Nakano, R. 1991 Vibration of a flexible plate weir due to the fluid discharge. In *Proceedings Asia-Pacific Vibration Conference* '91, pp. 10.13–10.18.

Kaneko, S., Nagakura, H. & Nakano, R. 1993 Analytical model for self-excited vibration of an overflow flexible plate weir. In *Flow-Induced Vibration and Fluid-Structure Interaction—1993* (eds M. K. Au-Yang & D. C. Ma), PVP Vol. 258, pp. 151–162. New York: ASME.

LU, D. 1995, Analysis of overflow-induced vibration of the weir coupled with sloshing in the downstream tank using physical component BFC method. Doctoral Thesis of the Faculty of Engineering, The University of Tokyo.

LU, D., TAKIZAWA, A. & KONDO, S. 1995a. Extension of PC-BFC method to the analysis of flows with free and moving boundaries. In *Proceedings First Asian Computational Fluid Dynamics Conference,* pp. 1167–1172, Hong Kong.

LU, D., TAKIZAWA, A. & KONDO, S. 1995b Analysis of overflow-induced sloshing in an elastic-wall vessel using physical component BFC method. In *Proceedings 7th International Meeting on Nuclear Reactor Thermal-Hydraulics* (*NURETH-7*), pp. 1302–1312, Sarantoga Springs, NY, U.S.A.

TAKIZAWA, A., KOSHIZUKA, S. & KONDO, S. 1992 Generalization of physical component boundary fitted coordinate (PCBFC) method for the analysis of the free surface flow. *International Journal of Numerical Methods in Fluids* **15,** 1213–1237.

TAKIZAWA, A. & KONDO, S. 1993 Development of physical component boundary fitted coordinate (PCBFC) method for the analysis of free surface flow. In *Proceedings International Conference on Nonlinear Mathematical Problems,* Vol. 1, pp. 1–16. Gakuto International.

APPENDIX: NOMENCLATURE

a or $a(\tau)$	exponential growth rate of the weir vibration
C_d	empirical coefficient for estimation of overflow rate
D	amplitude of forced vibration of the left wall
E	coefficient determined by the size of tank
F	coefficient determined by the size of tank
G	coefficient determined by the size of tank
GR	growth rate of sloshing
g	gravity constant
H	height of the weir
h	depth of the downstream tank
$h(t)$	thickness of overflow at top of the weir
I	moment of inertia of the wall (or weir)
k	spring constant
L	distance from the hinge to the spring
l	width of the tank
m	mass of the movable wall
p	pressure in the fluid
$q(t)$	overflow rate
q_0	constant part of overflow (inlet flow rate of the upstream tank)
T	period of sloshing
t	time
x	coordinate axis in physical space
z	coordinate axis in physical space
V	inlet velocity of the upstream tank
W	inlet width of the upstream tank
$\eta(t)$	water level of the free surface
$\theta(t)$	angle of the movable wall (or weir)
$\xi(t)$	displacement of the movable wall
τ	time delay
τ'	time by which the overflow is ahead of the weir vibration
ϕ	flow velocity potential
ω_b	natural frequency of the wall (or weir)
ω_n	natural frequency of sloshing in nth mode
$\omega_\pm$	two natural frequencies of the fluid-wall coupled system